DEPARTMENT OF DEFENCE

DSTO

Communications Division

RESEARCH REPORT
ERL-0673-RR

ELECTRO-OPTIC CHARACTERISATION OF EXTREMELY WIDE BANDWIDTH ELECTRICAL SIGNALS

by

A.C. Lindsay, G.A. Knight, S.C. Troedson and I.G. Fuss

ELECTRONICS RESEARCH LABORATORY

APPROVED FOR PUBLIC RELEASE

AR-008-114

DSTO AUSTRALIA

ELECTRONICS RESEARCH LABORATORY

Communications Division

RESEARCH REPORT
ERL-0673-RR

ELECTRO-OPTIC CHARACTERISATION OF EXTREMELY WIDE BANDWIDTH ELECTRICAL SIGNALS

by

A.C. Lindsay, G.A. Knight, S.C. Troedson and I.G. Fuss

SUMMARY

In this report an ultrafast electro-optic sampling system suitable for applications such as device characterisation is described. The aperture time of the sampler is calculated to be about 290 fs, implying an attainable device bandwidth in excess of 300 GHz. The sampler was characterised using a test pulse with approximately 12 GHz of frequency content, and the results compared to those obtained from an 18 GHz digital sampling oscilloscope.

FEB 93

APPROVED FOR PUBLIC RELEASE

POSTAL ADDRESS: Director, Electronics Research Laboratory, PO Box 1500, Salisbury, South Australia, 5108.

CONTENTS

FIGURES

APPENDICES

1 INTRODUCTION

It is becoming increasingly difficult for electronic technology to adequately cover the full electromagnetic environment that is of interest to communications countermeasures. Apart from the traditional HF spectrum, developments such as modern millimetre wave technologies, spread-spectrum techniques such as frequency hopping and discrete sequence are driving surveillance receivers towards large bandwidths. Commensurate with this is the fundamental requirement for instrumentation capable of efficiently and accurately characterising the electronic components and materials required by the expanding signal environment. In this report, an electro-optic ultrafast sampling system is described [1]. The system as demonstrated is, in its most basic form, a jitter-free 300 GHz bandwidth sampling oscilloscope. The fact that the system is jitter-free means that the Fourier transform of the signal contains accurate phase information over the full 300 GHz band and as such the demonstrator has the capability of a 300 GHz vector network analyser.

In section 2 a brief discussion of the ultrafast laser system is given. The two broad categories of sampling problems to which the research may be applied are defined. In section 3, the experimental set-up is described and in section 4 the results discussed. Finally, in section 5 applications of the technique and future research directions are summarised. Details of the theory of operation of the optical modulator are given in Appendix A.

2 FEMTOSECOND LASERS AND ULTRAFAST SAMPLING

The ultrafast laser system used in this work is a commercially available tunable dye laser pumped by a neodynium:YAG (Nd:YAG) solid state laser (YAG is an acronym for yttrium, aluminium and garnet). The laser output is tunable over a frequency range determined by the type of organic dye used as the lasing medium in the dye laser, however in this work the wavelength is constant at ~ 648 nm (at the red end of the visible spectrum). Pulses of the order of 120 femtoseconds (1fs = 10^{-15}s) at a repetition rate of 76 MHz are produced with a typical average beam power of 200 mW (19 kW peak pulse power). Pulses from ultrafast lasers based on similar general principles have achieved pulse widths of 6 fs [2] and as such represent the fastest controlled man-made phenomena in the world today.

When addresing the attainable bandwidths of competing technologies, it is against such timescales that the performance of particular sampling architectures must be measured.

It is useful to separate the sampling applications of ultrafast lasers into two broad categories. These are essentially "instrumental" applications and "one-shot" applications.

In the case of "instrumental" applications, the system is being used as an ultra-wide bandwidth oscilloscope or spectrum analyser. Thus the electrical signal being analysed is triggered repetitively by an optical pulse and then probed by an optical pulse. Both the

trigger pulse and probe pulse are initially derived from the same input pulse via a simple beamsplitting arrangement. The response at a given time instant (as sampled by the probe pulse) is averaged over millions of samples to obtain an acceptable signal, and then the probe pulse is delayed to a later time Δt and the process is repeated. In this way the waveform is gradually reconstructed in a similar manner to that in which most multi-gigahertz digital sampling oscilloscopes operate. An important consequence of the optical technique is that there is no contribution to measurement jitter from the measuring system itself, in contrast to electronic technology.

The "one-shot" application is much more difficult. In this case the pulse is used simply to construct an ultrafast optoelectronic sampling gate with a sampling rate of 76 MHz. The electrical signal is not repetitive, nor generated or triggered by the optical system. The reason for going to femtosecond aperture times is demonstrated by considering the aperture time constraint for analogue-to-digital conversion [3]

$$\tau < \frac{1}{2^n \pi B} \qquad (1)$$

or

$$\tau < \frac{1}{2^{DR/6} \pi B} \qquad (2)$$

where
- τ is the aperture time
- n is the number of bits in the digitiser
- DR is the dynamic range
- B is the signal bandwidth.

If very high dynamic range and/or wide bandwidths are required, then the aperture times rapidly become sub-picosecond. As an example, if it is required to digitise a 100 MHz bandwidth and retain a 70 dB dynamic range, Equation (2) gives $\tau \leq 1$ps. Any requirement for greater bandwidth or higher dynamic range constrains the aperture time to the femtosecond regime. Implementation of a "one-shot" sampling system that is capable of achieving large dynamic range is a much harder goal than the "instrumental" application, however it *is* the ultimate aim of the research. This report deals with our first attempt at ultrafast electro-optic sampling and details the construction of a sampler suitable for "instrumental" applications.

3 ELECTRO-OPTIC SAMPLING SYSTEM

3.1 The Electro-Optic Modulator

3.1.1 Basics of Operation

The basis of the sampling system is the electro-optic modulator, a schematic of which is shown in Figure 1. The electrical signal to be sampled is launched

onto coplanar stripline (CPS) which is deposited onto an electro-optic substrate - in this case the crystal lithium tantalate ($LiTaO_3$). The electric field penetrating the substrate between the coplanar strips induces in a change in the refractive index of the crystal, which in turn will alter the polarisation state of laser light passing through the crystal. As detailed in Appendix A, the addition of a 45° polariser before the modulator, along with a Soleil-Babinet compensator and crossed polariser after the modulator, results in a transmitted laser intensity which varies approximately linearly with the electrical signal. Thus, the characteristics of the electrical signal propagating along the CPS are reproduced as intensity variations of the laser beam.

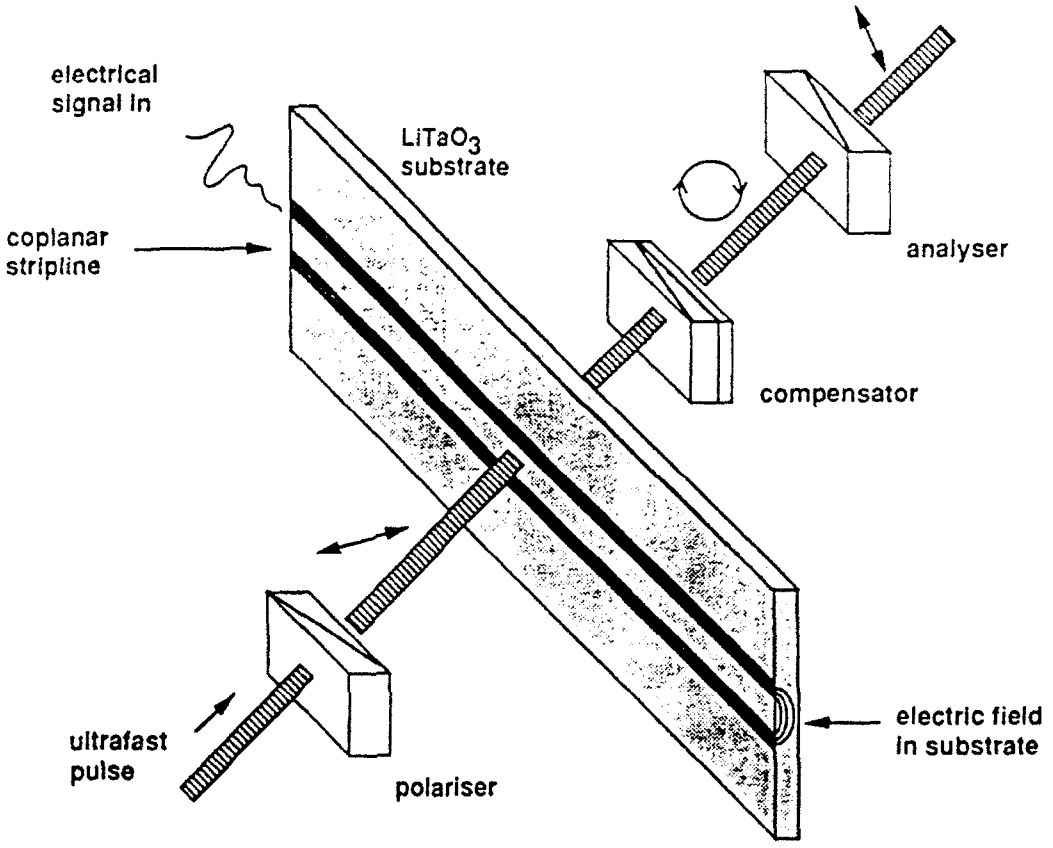

Figure 1 **Basis of the electro-optic sampler. The arrows indicate the evolution of the polarisation state of the laser probe.**

3.1.2 Construction Details

The unpolished $LiTaO_3$ crystal used as the electro-optic substrate was purchased from Crystal Technology Inc. The sample measured 1 mm(x) x 12.8 mm(y) x 25.4 mm(z), where x, y and z refer to the crystallographic axes. The crystal was polished by the Adelaide-based company Jung Precision Optics.

Gold coplanar stripline (CPS) electrodes 50 µm wide with a gap of 50 µm were deposited along the y direction of the crystal so that the field between the CPS was directed along the z crystal axis. Using closed-form expressions [4, 5] the calculated impedance of the structure was 51 Ω.

A launch structure was fabricated to launch the electrical RF signal from the coaxial feed cable onto the CPS with minimal electrical mismatch and mechanical stress (since the crystal is easily damaged). The launcher incorporates a Cascade Microtech EL26 adaptor to launch from coax to coplanar waveguide (CPW). A constant-impedance taper is then used to transform the CPW to CPS. The taper was fabricated using planar techniques on a 12.7 mm wide, 635 µm thick alumina substrate. The launch substrate was mounted alongside the crystal on a brass carrier block with electrical connection being made by bond wires. A second "reverse" output launch substrate was mounted on the other side of the crystal to make transmission measurements possible. A hole was machined through the carrier under the middle region of the crystal to leave a path for the laser. The carrier block also provided holes for attaching the EL26 adaptors.

The 25.4 mm length of the crystal allowed for several launch designs (including some with resistive terminations) to be tested side-by-side and to provide redundancy. Figure 2 shows an overlay outline plot of the art work for the two launch substrates and the crystal. The designs were essentially combinations of single and double sided taper to transform from the CPW mode to the CPS mode required by the sampler. The results given in this report are those obtained using the two-sided taper design with no resistive termination.

The electrode design and layout were undertaken by Electronic Warfare Division (DSTO), with the electrode fabrication and bonding being performed by Microelectronics Section (DSTO).

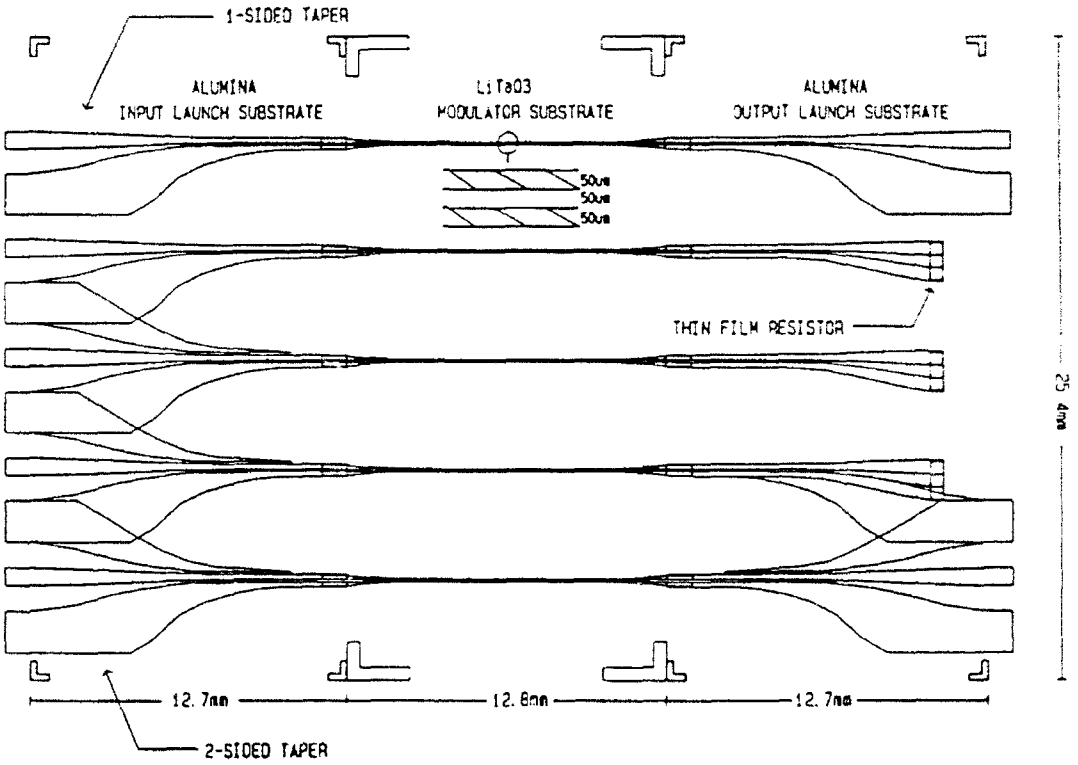

Figure 2 **Outline plot of the coplanar electrode structures. The two-sided taper design was used for the work reported in this document**

3.2 Optical Layout

A schematic of the experimental layout is shown in Figure 3. An incoming 120 fs duration optical pulse is split into a trigger pulse and a probe pulse. The trigger pulse is used to trigger the ultrafast electrical signal, which in this experiment was obtained originally as the impulse response of a fast photodiode (photodiode D1 in Figure 3).

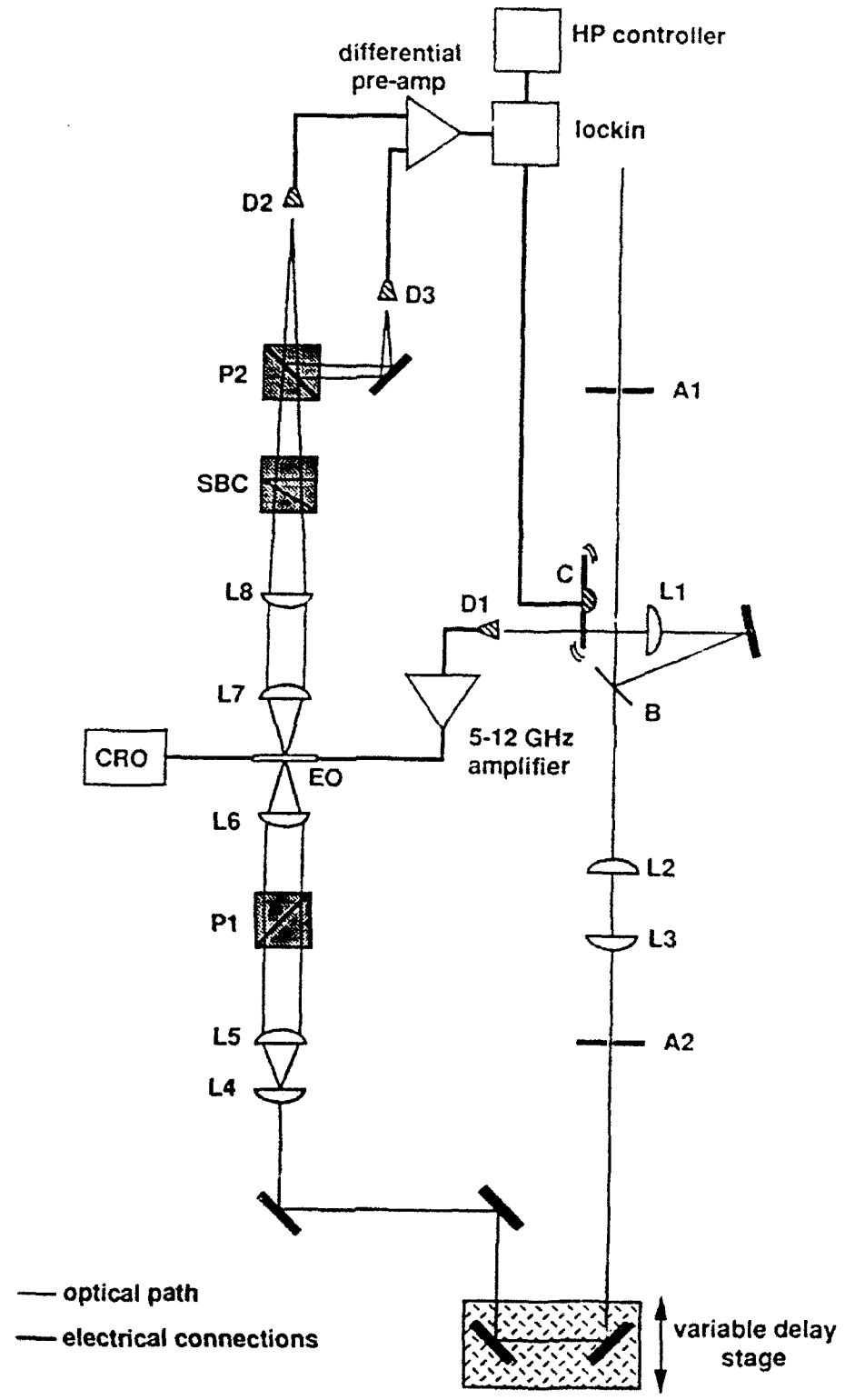

Figure 3 **Experimental layout**

The probe pulse is delayed via a 2 µm resolution variable delay line and brought to an ~18 µm diameter focus between the CPS carrying the electrical signal. The delay is initially adjusted so that the probe pulse arrives at the $LiTaO_3$ sampler a few tens of picoseconds prior to the triggered electrical signal. The computer controlled variable delay can then be increased in a stepwise manner, which results in the probe pulse "scanning" the electrical waveform. At each step many millions of samples are averaged (as described in section 3.4) to obtain a good signal-to-noise ratio. Since the trigger pulse and probe pulse are originally derived from the same optical pulse, and the delay is determined by the physical propagation path followed by the probe, exactly the same point on the electrical waveform is sampled at each given step of the variable delay. This has the important consequence that the sampling process is essentially jitter-free, and thus the Fourier transform of the sampled signal will contain accurate phase information across the full bandwidth. The very small amount of jitter that does exist is determined by the vibration of the beam steering mirrors on the optical bench. As an example of how small this contribution is, a mirror surface in the delay path would have to move ±15 µm to result in a timing jitter of ±100 fs. Motion of ±15 µm is quite a large excursion for a solid optical component mounted on a vibration-isolated optical bench.

The following list details the optical components shown in Figure 3 and their role in the experiment:

A_1, A_2 iris diaphragm apertures - define the height and alignment of the incoming optical beam. This minimises daily re-alignment of the optical layout.

B variable circular beamsplitter - allows variable ratio of trigger pulse intensity to probe pulse intensity.

C chopper wheel - provides a modulation for the lock-in amplifier. This is described fully in section 3.4.

D_1 40 ps rise time fast photodiode.

D_2, D_3 general purpose photodiodes.

EO $LiTaO_3$ electro-optic modulator.

L_1 focussing lens to ensure small laser beamwidth at chopper (to get a clean square wave), and to get efficient coupling of the laser onto the fast photodiode.

L_2, L_3 beam handling lenses to minimise beam divergence.

L_4, L_5 beam expanding lenses to allow final focussing to ~ 18 µm.

L_6, L_7 focussing and re-collimating lenses.

L_8 long (250 mm) focal length lens to focus beam onto detectors D2 and D3.

P_1, P_2 Glan-Thompson polarising beamsplitters.

SBC Soleil-Babinet compensator - to remove $LiTaO_3$ birefringence and produce quarter-wave retardation between the vertical and horizontal polarisation components of the laser beam (as discussed in Appendix A).

3.3 Generating the test signal

As noted in Section 3.1, the electrical test signal used in this demonstrator was derived from the impulse response of an Opto-Electronics Inc PD15 fast photodiode. This signal, as recorded by an 18 GHz bandwidth HP54120B digital sampling oscilloscope, is shown in Figure 4. The rise time of the pulse is approximately 37 ps and the width is about 74 ps. Initially, this pulse was launched directly across the $LiTaO_3$ modulator.

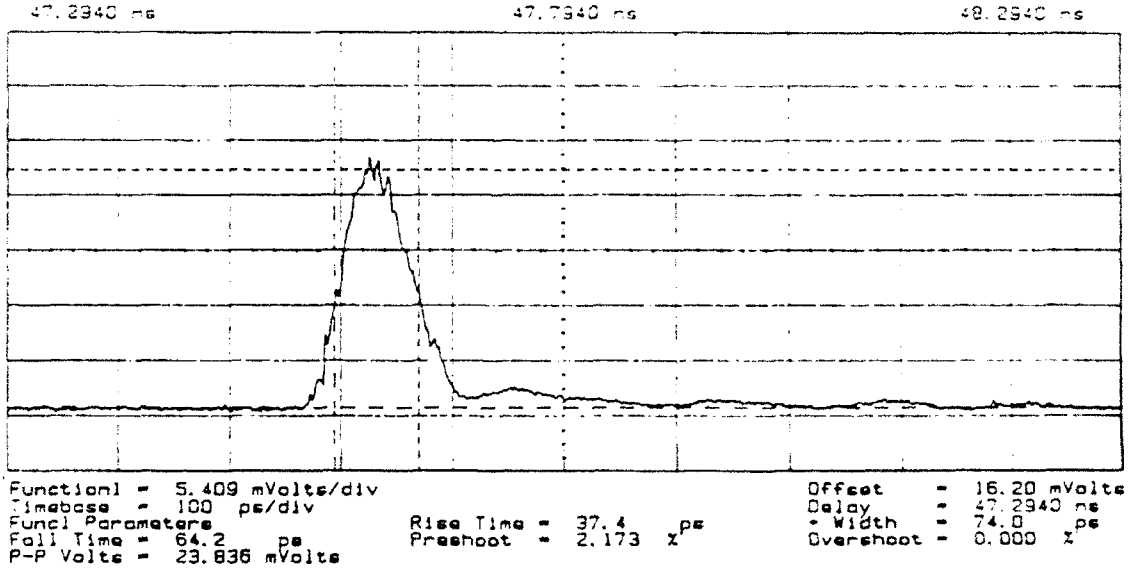

Figure 4 Impulse response of the PD15 fast photodiode

It was found, however, that the signal was too small to be easily detected while the experiment was being optimised, and as such the pulse needed to be amplified. The only amplifier readily available was a Watkins-Johnson WJ-6884-824, 5-12 GHz, 30 dB gain bandpass amplifier. The result of amplifying the photodiode output pulse of Figure 4 with this amplifier is demonstrated in Figure 5. While this final pulse has significant ringing structure lasting over 700 picoseconds, the peak-to-valley spacing of the significant features of the leading edge of the signal still occur on a timescale of about 30 ps, and as such it is no worse a test signal than the original pulse. In fact, the final pulse is significantly more interesting since comparison of the actual shape of the various features as measured by the 18 GHz oscilloscope and the electro-optic technique will give some qualitative indication of the effect of timing jitter on determining the true signal shape.

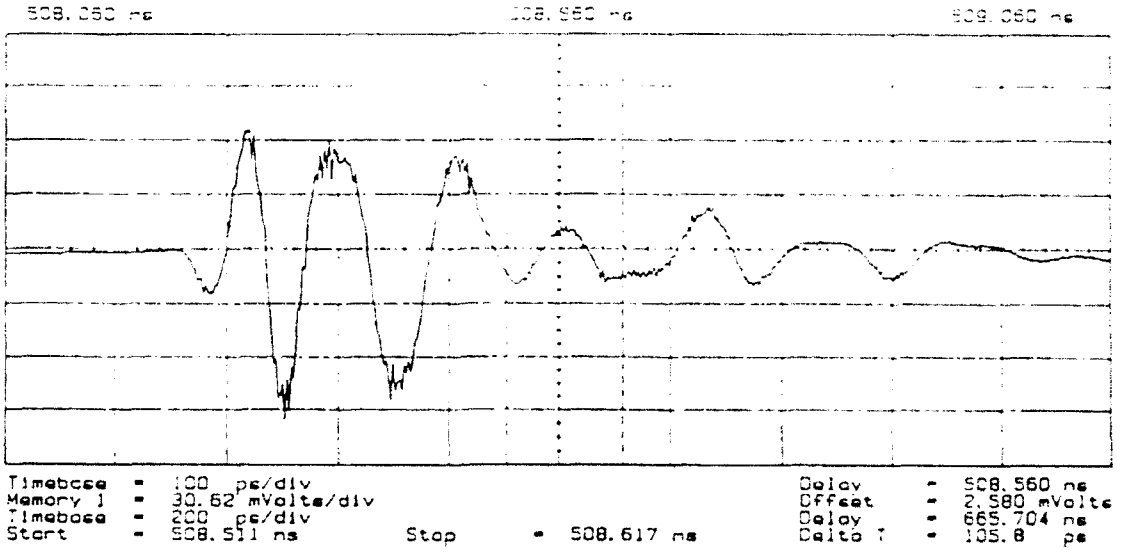

Figure 5 Effect of the 5-12 GHz bandpass amplifier on the pulse shown in Figure 4

As described in Section 3.1.2, the test signal was coupled onto the launching structures of the modulator via EL26 adaptors. From these the mode structure of the pulse evolves into a quasi-TEM mode which propagates across the modulator and then on to the 18 GHz oscilloscope via the reverse arrangement to that used to launch the signal. All cabling connecting the photodiode, amplifier, modulator and oscilloscope was rated to 26 GHz and caused no measurable dispersion of the pulse shown in Figure 4.

3.4 Detection System

The change in refractive index of the $LiTaO_3$ crystal due to the electrical signal is expected to be extremely small. For our samples, a 1V amplitude would lead to a change of the order of only $\sim 10^{-6}$ in the refractive index. Thus, a lock-in detection system must be used to detect the signal.

The chopper shown in Figure 3 chops the triggering pulse train at a known frequency (typically 1.48 kHz), and provides a reference signal at the same frequency to a PARC 5301A lock-in amplifier. Since the electrical signal is being chopped, a corresponding modulation will appear on the optical pulses sampling the refractive index variation of the $LiTaO_3$ substrate. The signal current from detectors D2 and D3 are separately pre-amplified by UDT101C transimpedance amplifiers (not shown in Figure 3) and then differentially detected by a PARC 5316 differential pre-amplifier, with the differential output providing the signal to the lock-in.

Differential detection allows a simultaneous removal of spurious noise and a doubling of the detected signal voltage i.e. a 6 dB increase in detected signal power.

The lock-in amplifier has selectable time constants which allow signal averaging from 1 ms to 100 s. For this work exponentially weighted averaging using time constants ranging from 300 ms to 30 sec were employed.

4 EXPERIMENTAL RESULTS

4.1 Electrical Characterisation of the Modulator Design

The microwave performance of the assembled sampler was characterised over a 20 GHz bandwidth using a Wiltron 360 Vector Network Analyser. The S-parameters magnitude versus frequency plots are shown in Figure 6. These results are for the 2-sided taper design, although it was only marginally better than the 1-sided taper design. The S21 transmission coefficient indicates the network has an average of 10 dB loss across the band and the S11 reflection coefficient shows a return loss of 15 dB.

As indicated by a low value of S11 there was minimal reflected power (some 3%) from the terminals of the assembled sampler (S11 only indicates what is reflected at the measurement terminals) so a good match was provided to the external setup.

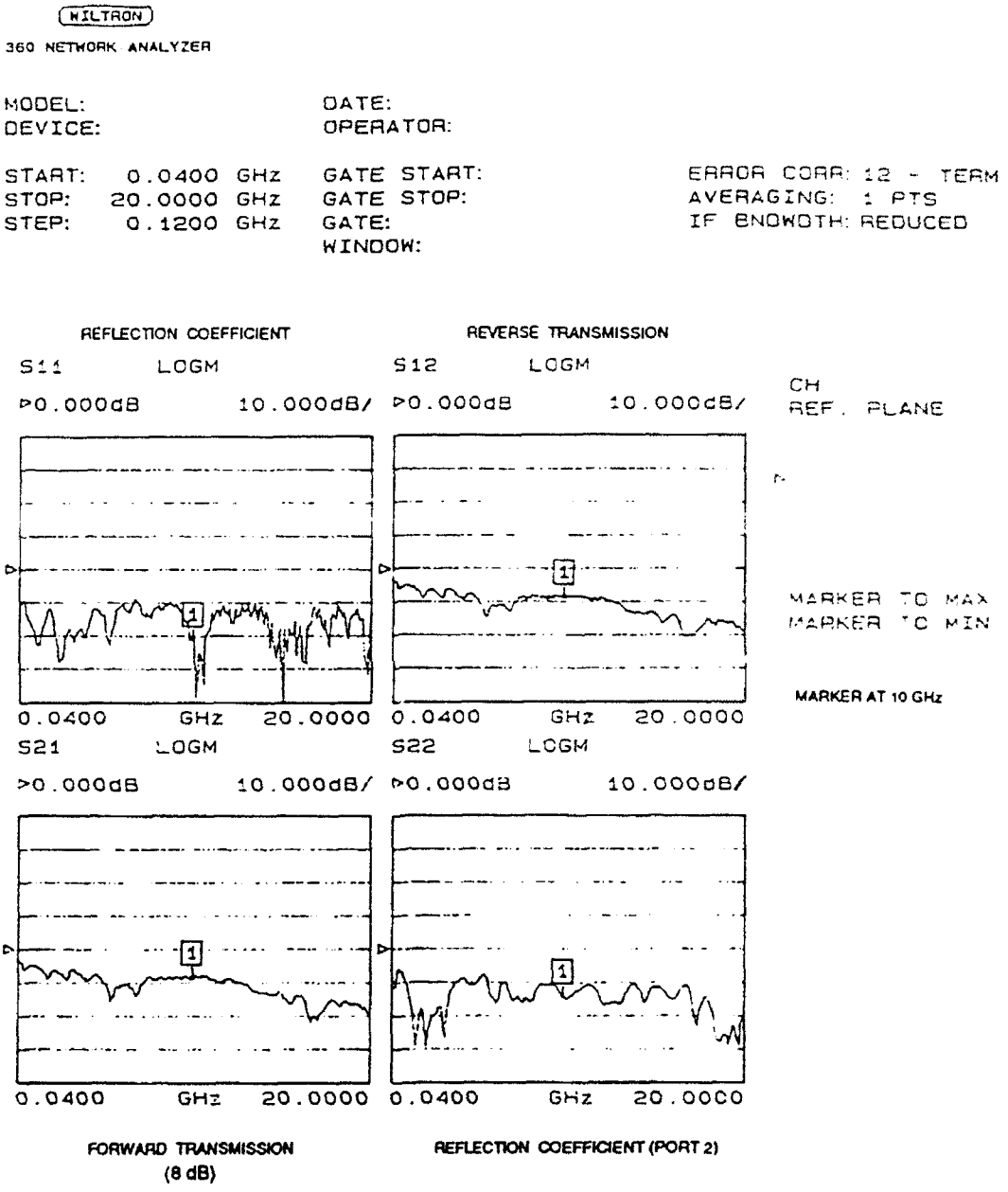

Figure 6 **Microwave performance of the assembled sampler**

The major sources of loss of transmission power are not well understood at this stage. Since power is not reflected at the terminals it must either be absorbed within the network or radiated. A significant portion of the 10 dB loss (at least 3 - 4 dB) can be attributed to the high resistivity of the modulator and launcher conductors. At the time of fabrication gold could only be deposited to a thickness of about 0.2 μm which meant that the conductors had a total resistance (from input to output) of up to 50 Ω and hence high resistive losses. The ripples in the responses tend to indicate that some of the power is lost into non-TEM modes (high order modes, surface-wave modes etc). These non-TEM modes can be launched from any of the discontinuities within the network and are radiated, absorbed or reflected back into the network. There is also the normal attenuation increase versus frequency that occurs with all types of physical transmission lines, especially coplanar lines which have current crowding at the edges of the conductors, resulting in high resistive losses - these effects have not yet been investigated for this structure.

Another electrical parameter of interest is the dispersion characteristic of the stripline structures. This was obtained by bypassing the 5 - 12 GHz amplifier and using the sampling oscilloscope to measure the shape of the electrical pulse from the fast photodiode, with and without the modulator structure in the propagation path. These results are shown in Figures 7(a) and 7(b) respectively. As can be seen, the full width of the pulse at half maximum voltage is essentially unchanged, however, the rise time has increased from 37 ps to approximately 78 ps, and a significant psuedo-exponential tail of some 200 ps duration with some ripples is apparent. The increased rise time can be attributed to dispersion experienced by the pulse as it propagates across the modulator structure. The long tail is a combination of the effects of dispersion and of multiple reflections due to impedance mismatches between the couplers, launchers, bond wires and coplanar stripline sections of the modulator structure.

It is clear that accurate time domain reflectometry (TDR) would give a useful insight into the above observed performance. Unfortunately, due to dispersion and the high resistivity of these transmission lines, meaningful TDR has not been possible. In the future however, with calibration on the Wiltron 360 for coplanar structures (and hence correction for dispersion) and a re-fabricated sampler with thicker gold lines, it should be possible to undertake meaningful TDR.

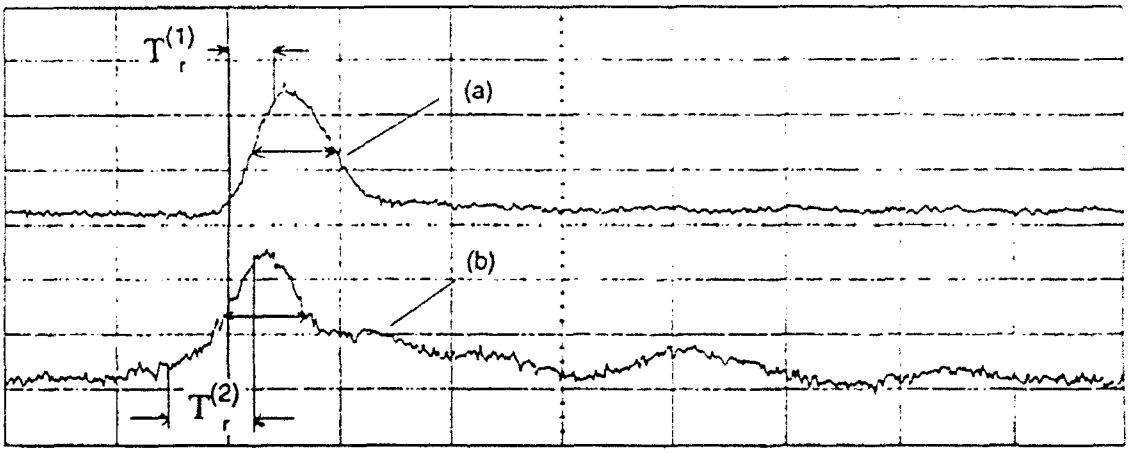

Trace (a): input pulse to e - o sampler
Trace (b): output pulse after sampler (1mv / div)

Figure 7 **Demonstration of pulse dispersion due to the sampler. Trace (a) shows the pulse input to the sampler, trace (b) shows the output pulse.**

4.2 Electro-Optic Sampler Performance

4.2.1 Signal Sampling

The result of electro-optically sampling the first 400 ps of the test signal of Figure 5 is shown in Figure 8. For comparison, Figure 9 shows the same section of the signal as measured by the sampling oscilloscope with 128 averages per point. The data points in Figure 8 correspond to a time between samples of 4 ps and an exponentially weighted, 300 ms integration time on the lockin detector was used.

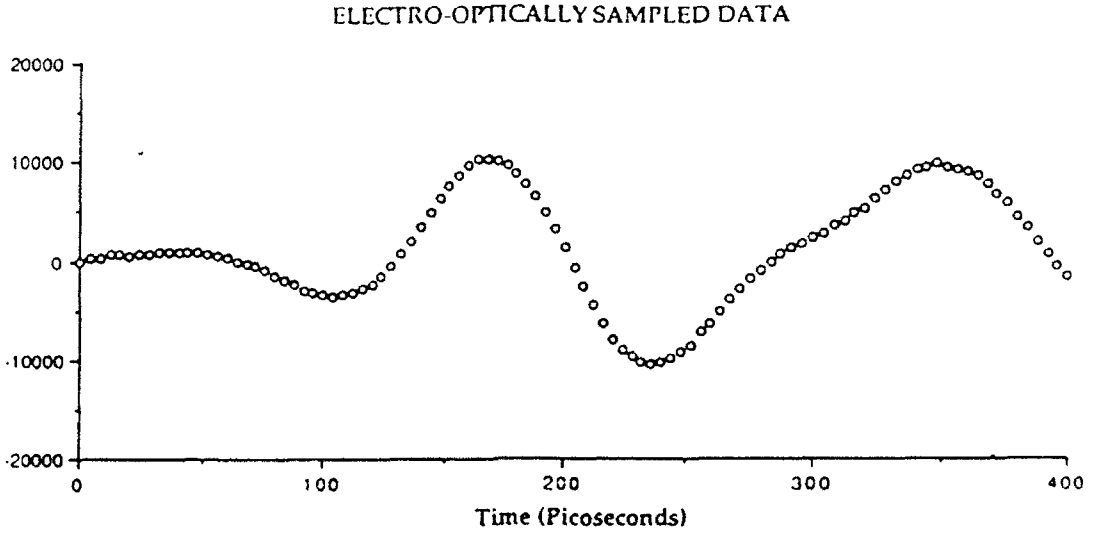

Figure 8 **The first 400 ps of the test signal shown in Figure 5, obtained by electro-optic sampling**

The approximate peak separation as measured by the electro-optic sampler is 184 ps. This compares well with the estimate from Figure 9 of about 181 ps.

The major differences between the traces are the amount of noise and the variation in the ratio of the amplitudes of the peaks and troughs of each trace. The significantly greater signal to noise ratio of the data from the electro-optic sampler is due to the substantially greater averaging that can be readily achieved. The fundamental sampling rate of 76 MHz and integration time of 300 ms implies that an exponentially weighted average of about 23 million samples contribute to each point of the final signal (a factor of 2 arises due to the fact that the optical trigger pulse is being chopped). In the case of the oscilloscope signal, typically only 128 samples were used.

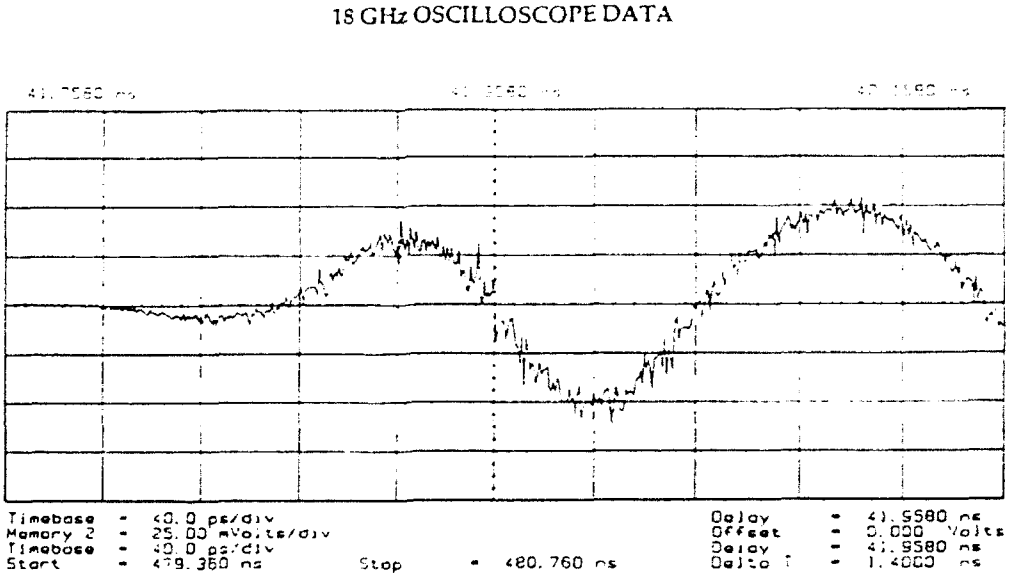

Figure 9 **The first 400 ps of the test signal shown in Figure 5, obtained using the 18 GHz digital sampling oscilloscope.**

The variation in the ratios of the amplitudes of the various features that can be seen when comparing Figures 8 and 9 has several possible origins. A definite contribution will arise through the "smearing" effect of timing jitter on the oscilloscope signal. The trigger for the oscilloscope was derived from the signal used to mode-lock the Nd:YAG laser (mode-locking is the process which results in the Nd:YAG laser producing pulses rather than a constant beam). This means that the oscilloscope trace is subject to both pulse-to-pulse jitter due to the laser source and the usual timing jitter associated with its own electronics. The smearing effect would be expected to be greater for features of short duration and would result in an overall reduction of the real amplitudes due to the averaging.

Figure 10 shows a histogram of the timing jitter of the laser pulse as recorded by the digitising oscilloscope. The histogram was built up over 60000 samples, and the standard deviation is measured to be 19 ps, most of which is attributable to pulse-to-pulse jitter associated with the laser system (the trigger for the digitising oscilloscope is specified to have a standard deviation jitter value of about 2 ps).

In order to check the effect of timing jitter, the signal recorded by the electro-optic sampler, Figure 8, was mathematically "jittered" by generating a Gaussian distributed random time offset with selectable standard deviation. A cubic spline interpolation routine was then used to estimate the new signal amplitude at each original data point. A number of such signals (typically 128) were then averaged to generate the "jittered" signal. Finally, a 5% random noise (roughly equivalent to the noise level observed in Figure 9) was added to the signal.

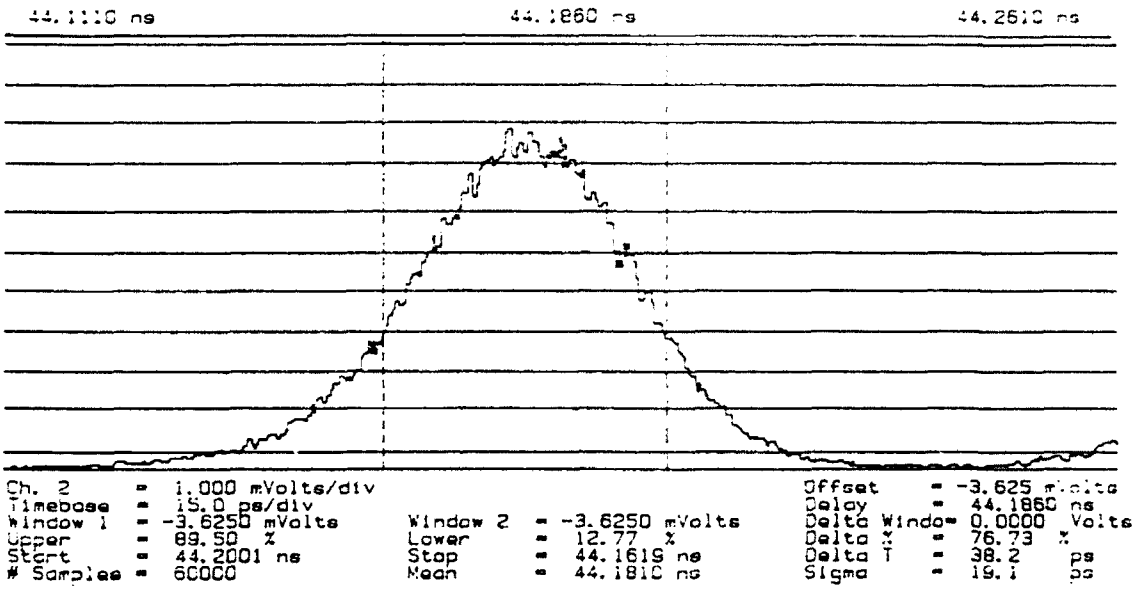

Figure 10 **Measurement of the timing jitter associated with the laser pulse and oscilloscope electronics.**

Figure 11 demonstrates the result of carrying out this simulation using 128 traces and a 19 ps jitter, as suggested by the histogram of Figure 10. It is apparent that the features are somewhat "washed-out", as is expected, and the slightly shorter duration features have been slightly more effected than the slower, final peak. The asymmetric feature near the top of the final peak (apparent in Figure 8, but not in Figure 9) has also been removed. However, the variations are not large enough to fully account for the differences between Figures 8 and 9.

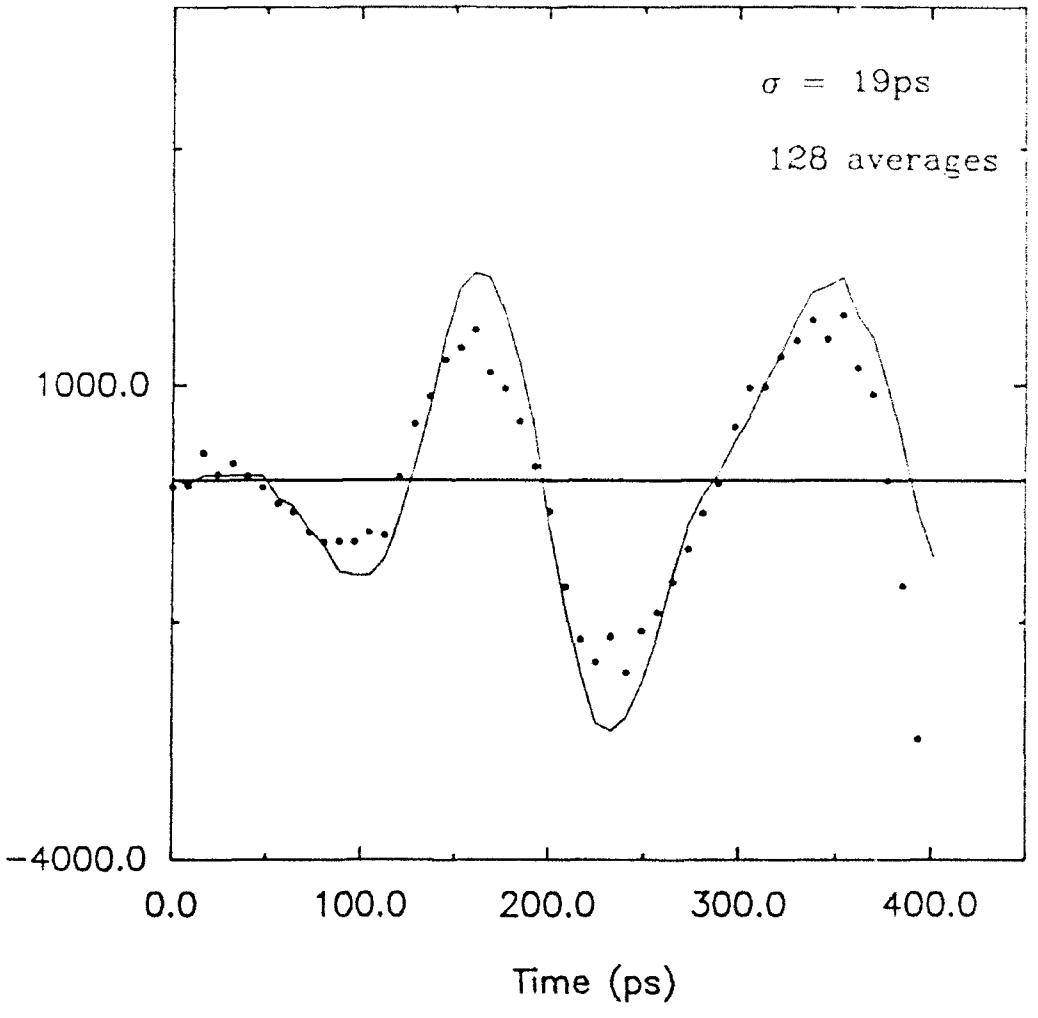

Figure 11 **Simulation of the effect of timing jitter and noise. The solid line represents the original electro-optic samples, the dots show the result of subjecting these samples to Gaussian timing jitter with σ = 19 ps and 5% noise.**

A second possible explanation for the different amplitudes lies in the possibility that the modulator was improperly biased. As demonstrated in Appendix A, the response of the modulator is in fact sinusoidal, but it should be optically biased to the linear region at zero volts. If the modulator were inadvertently biased substantially far from the linear region a non-linear response could result.

This second possibility for the difference between the traces is unlikely, due to the large switching voltage of $LiTaO_3$, which is ~ 2 kV (the switching voltage is the voltage required to induce a phase change of π in the modulator reponse, as discussed in Appendix A). Since the peak-to-peak voltage difference is no more than 1 V, only about 1/2000 of the sinusoidal transfer function is used. Thus, while being biased in the linear region will be most efficient (since the derivative is greatest), the very small region of the transfer function actually used will probably be "sufficiently linear" so that any non-linear response is negligible. The fact that the modulator is biased very near to its linear region is also supported by the dynamic range results, which are discussed in the next section. Furthermore, it would be expected that the non-linearity be apparent in both oscillations of the signal, and not just in the final peak. Thus, it is extremely unlikely the transducer non-linearity is the cause of the observed discrepancy.

Other possible contributions are the effects of dispersion and multiple reflections between the end of the CPS and the SMA connectors at the output, which will only alter the signal *after* the electro-optic measurement, or simply the possibility of the estimation routines in the digitising oscilloscope being biased. The former conjectures are the most likely, since in the transition region of the launcher the propagation mode must evolve from the CPS mode to the CPW guided mode and then finally to the propagation mode of the coaxial cable. This process could very well be the main source of significant dispersion (and loss) in the structure, and as such could account for the differences in the measured signal.

In order to try to obtain further insight into the discrepancies between the recorded signals, the Fourier transform of both the electro-optic measurement and the oscilloscope measurement were calculated and compared. The results are shown in Figure 12. It is immediately apparent that there appears to have been an almost "resonant" loss process slightly above the 10 GHz region. This is the sort of loss that could be due to the transition regions of the launchers. A comparison of the reflection coefficients of ports 1 and 2 (the input and output launchers) as recorded by the vector network analyser - as shown in Figure 6 - suggests that the output launcher is somewhat less well matched than the input launcher in this region. Thus, it is possible that while there is good coupling of the input launcher to the sampler in the region immediately above 10 GHz, there may be loss at the output launcher.

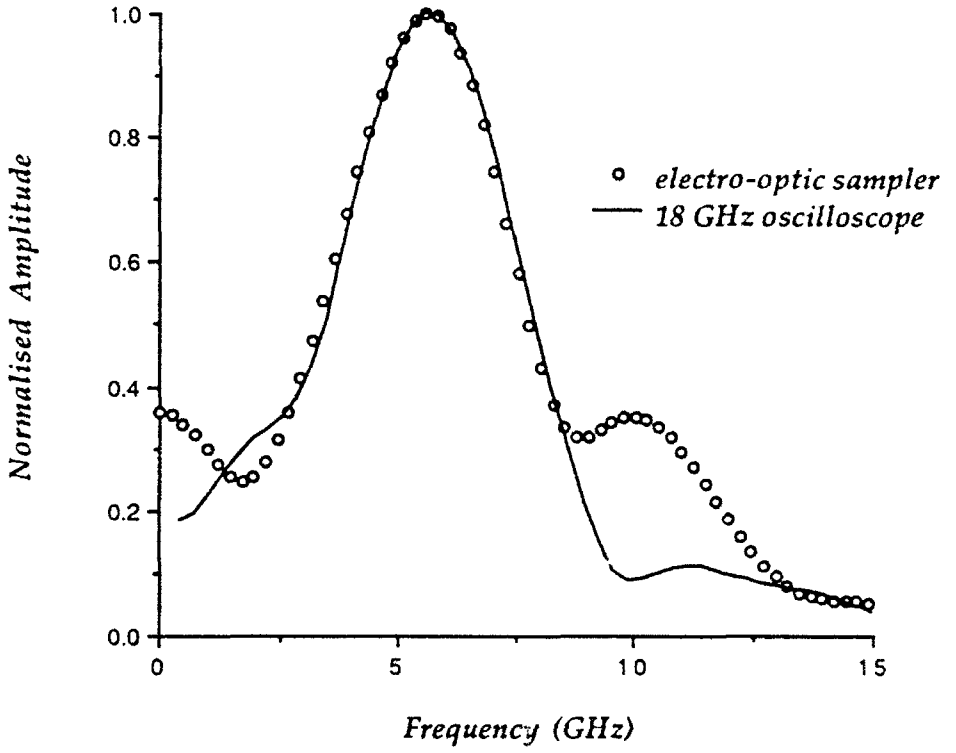

Figure 12 **Comparison of the Fourier transform of the electro-optically sampled signal with that of the digitally sampled signal.**

As discussed in section 4.1, the exact sources of significant dispersion, reflection and loss can only be determined by careful TDR analysis of the modulator structure.

4.2.2 Sensitivity, Dynamic Range and Insertion Loss

The ultimate sensitivity of the modulator is a strong function of the amount of signal averaging performed by the lock-in amplifier. In order to establish the sensitivity of the device a 1.48 kHz signal from the lock-in was used as the electrical signal applied to the modulator to directly modulate the probe beam. The resulting optical modulation was detected as a function of electrical power input to the modulator by the lock-in.

From Figure 6 a worst-case estimate for the sensitivity and insertion loss across an 18 GHz bandwidth can be inferred to be about 10 dBm down from the values measured at 1.48 kHz. In contrast, the dynamic range measurement

will accurately reflect the high frequency behaviour of the device, since the non-linearity of the modulator response is essentially independent of frequency.

The results are shown in Figure 13. From the figure the linearity of the device response is apparent, which indicates that the modulator was accurately biased. The data indicate a sensitivity of about -30 dBm (input) for which a 30 second integration time was necessary. The device was measured to have a linear response in excess of 60 dB, and a system insertion loss of ~ 64 dB.

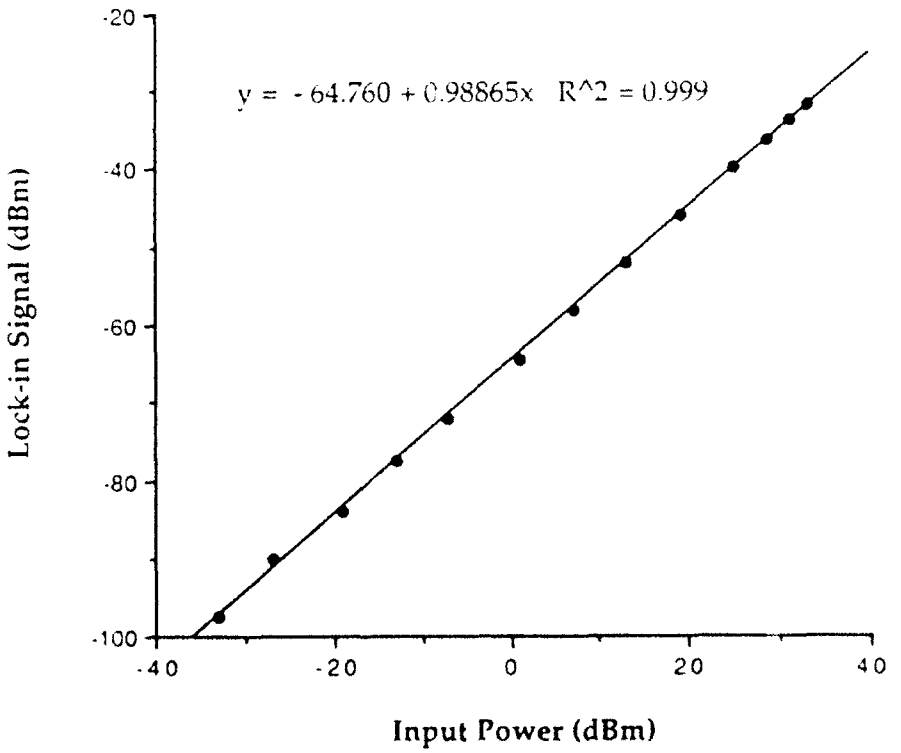

Figure 13 Characterisation of sampler linearity, sensitivity and insertion loss.

4.2.3 Aperture Time and Device Bandwidth

The actual aperture time (the time over which the sample is taken) of an ultrafast electro-optic sampler is given by two distinct contributions. The first is the finite time it takes the sampling pulse to transit the fringing electrical field while the electrical signal propagates past the sampling position - as shown in Figure 14a - and the second contribution arises due to the transit time of the electrical signal across the waist of the laser probe (the finite width of the probe physically covers a finite signal duration, as shown in Figure 14b).

(a)

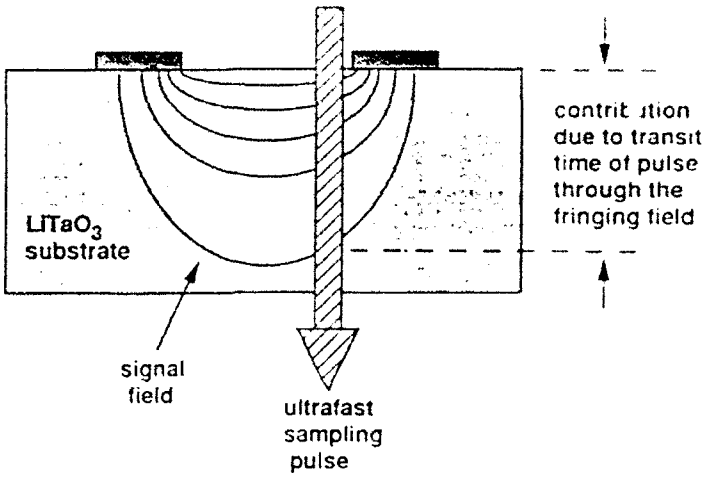

(b)

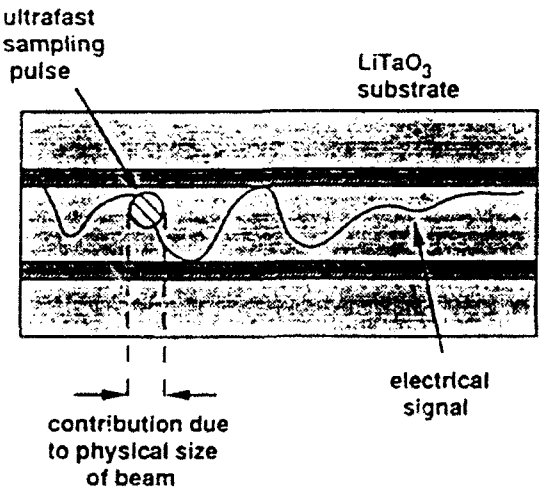

Figure 14 **Contributions to the aperture time of the electro-optic sampling process.**

Calculating the dynamic electric field distribution for the CPS configuration is a complex procedure which usually involves finite element or Green's function techniques. In order to do a simple "worst-case" calculation, a conformal mapping technique [6] was used to estimate the field distribution of a 1V amplitude static potential applied to semi-infinite electrodes separated by a 50 μm gap. The result of this calculation is shown in Figure 15. From this calculation, the field drops to 10% of its maximum at about 4 gap widths, or 200 μm. This corresponds to an interaction time of ~ 1.4 ps for the transit time of the pulse through the fringing field.

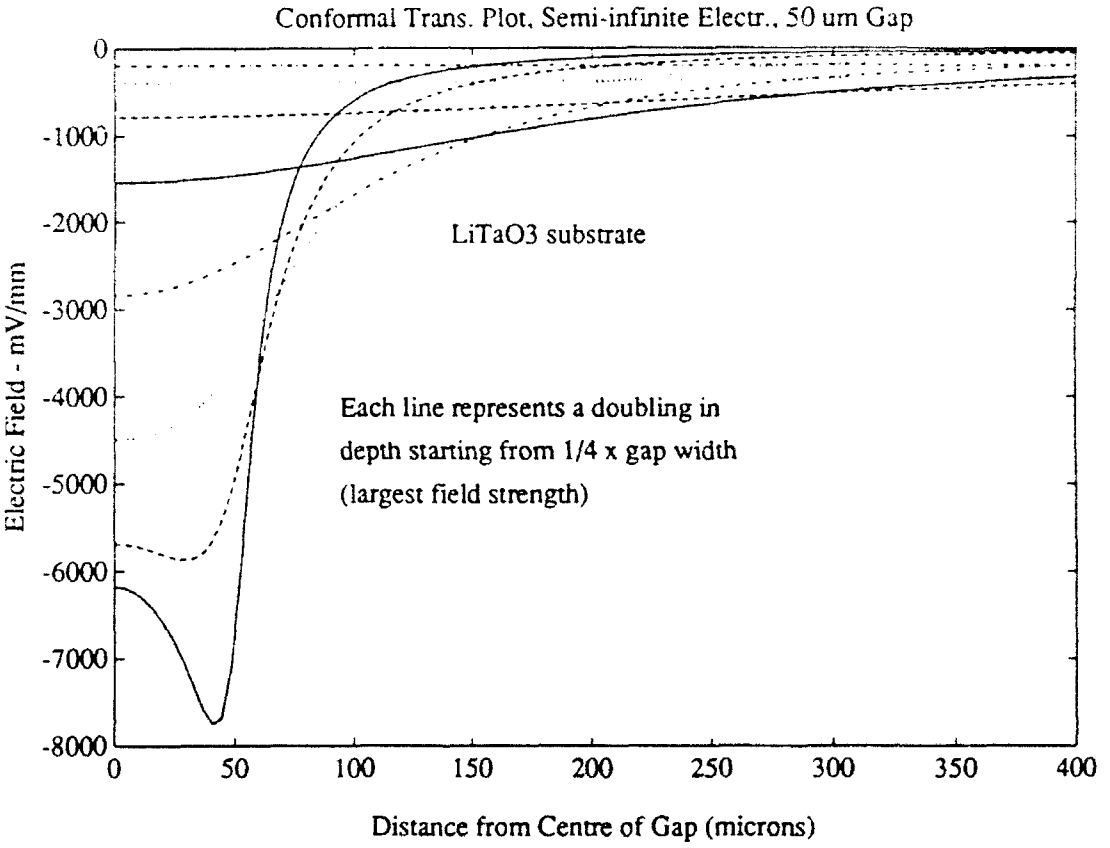

Figure 15 Static calculation of the approximate field distribution between the electrodes for a 1V static potential.

The second contribution to the total aperture time is the transit time of the electrical pulse through the beam waist. This quantity was measured by taking traces of the electrical signal at several positions along the electro-optic modulator and measuring the average delay of the electrical signal. From this a propagation velocity of 62.5 μm/ps was measured, which for an 18 μm beam waist corresponds to an interaction time of 290 fs.

From these measurements it is clear that the aperture time is dominated by the propagation time of the optical pulse through the fringing field and as such an estimate for the worst-case aperture time for the device is 1.4 ps. This aperture time is comparable to that obtainable using superconducting sampling techniques [7] or non-linear transmission line sampling techniques [8], which typically attain best performance results of about 2 ps.

A significant improvement can be obtained very easily simply by altering the interaction geometry such that the sampling pulse enters the crystal at an angle which ensures that the probe has a velocity component in the direction of electrical signal propagation equal to 62.5 μm/ps. In this *velocity-matched* configuration, the probe always "sees" the same part of the electrical signal and as such the aperture time is totally determined by the contribution due to the finite probe beam size. This reduces the aperture time to 290 fs, a figure which is not attainable by any other technology.

The ultimate bandwidth of the system will be determined by the aperture time, since the samples can be taken 7 fs apart if desired (due to the 2 μm resolution of the delay line). Since the aperture time is only 300 fs, it can be argued that the Nyquist frequency of the system is greater than 1 THz. However, it is more reasonable to use the criterion that the inverse bandwidth should ideally be at least an order of magnitude larger than the aperture time, which nonetheless still implies a device bandwidth easily exceeding 300 GHz. Due to the nature of the sampling process, this is, of course, not an *instantaneous* bandwidth.

5 APPLICATIONS AND FUTURE DEVELOPMENT

5.1 Component Characterisation

The particular type of electro-optic sampling system developed in this project is readily adapted for characterisation of extremely wide band or high frequency components such as HEMT transistors. A typical arrangement is shown in Figure 16. An ultrafast electrical pulse is generated by a photoconductive switch. A typical pulse would be 1-2 ps in duration. The pulse propagates along a small length of $LiTaO_3$, through the device under test (DUT) and along a second $LiTaO_3$ substrate to a matched termination.

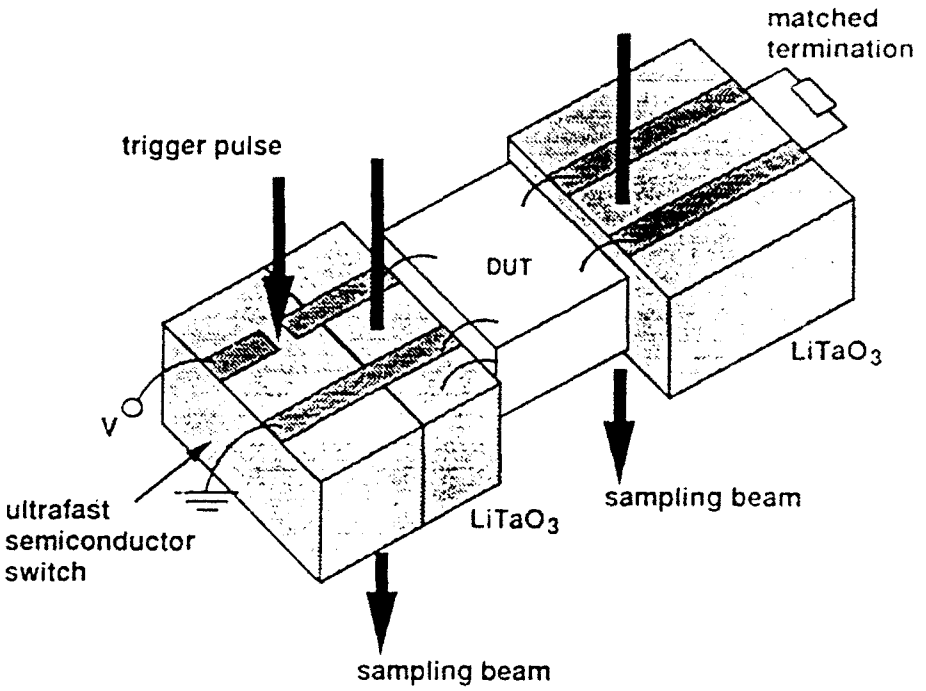

Figure 16 **Schematic of the experimental set-up used in electro-optic characterisation of microwave and millimetre components.**

The input and output pulses can be sampled electro-optically in the manner described in this report. Assuming the DUT has a linear response the output pulse will be the convolution of the input pulse with the response function of the DUT. Thus the complex transfer function of the device over several hundred gigahertz is readily determined using standard deconvolution techniques.

5.2 Materials Characterisation

A very similar experimental technique can be used to determine the complex dielectric function of new materials which, for example, may be necessary to construct radomes for extremely wide-band antennas. In this case the end section of the CPS is flared to produce a stripline antenna structure [9]. This launches the ultrafast electrical pulse into free space. An identical receiving antenna fabricated on a $LiTaO_3$ substrate is used to detect the pulse. Dielectric lenses can be used to collimate and re-focus the free-space

impulse to improve the coupling between the structures. The basic layout is shown in Figure 17.

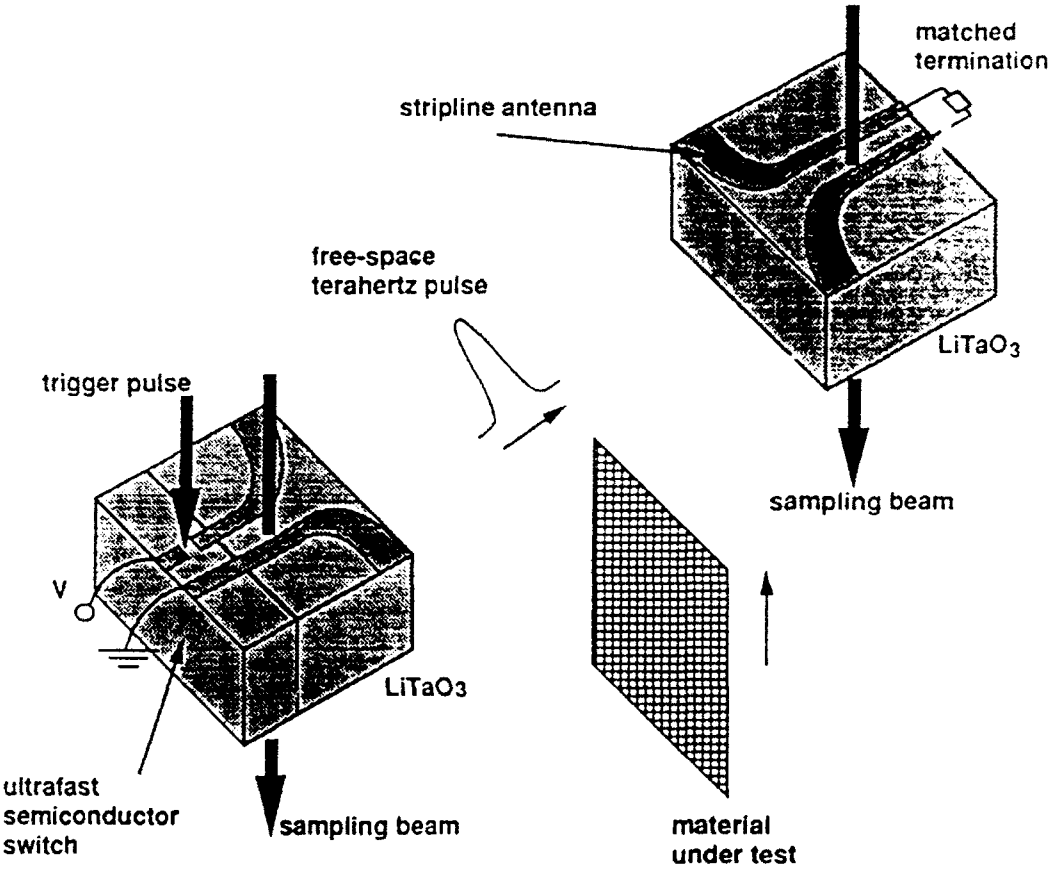

Figure 17 Schematic of the experimental set-up used in wideband materials characterisation.

Having measured the transmission characteristics of the system, the material to be investigated is then simply placed in the path of the pulse. The change in transmission characteristics will then allow the determination of both the real and imaginary parts of the dielectric function of the material over the full bandwidth of the sampling system.

This technique is known as COMITS (Coherent Optical Microwave Transient Spectroscopy) [9]. Placing wire polarizers on either side of the sample also allows orientational characterisation of the material.

5.3 Future work

The major component to construct and demonstrate during this work was the modulator structure. As described in Section 3.3, the signal generated by a fast photodiode was sufficient to demonstrate the capability of the device. For the applications described in Sections 5.1 and 5.2 however, an electrical pulse of picosecond or even sub-picosecond duration is required. Thus a program has been initiated to construct a semiconductor-based, sub-picosecond optoelectronic switch (known as an 'Auston switch). This project is progressing on two fronts:

(a) **MBE growth of low-temperature GaAs**

A program, has been undertaken in collaboration with CSIRO Division of Radiophysics, in which GaAs grown at low temperatures (~ 200°C) will be used as a photoconductive substrate to produce a sub-picosecond switch [10]. The sample has been supplied and a new lift-off technique is being attempted in order to lift the 2 nm layer of LT-GaAs.

(b) **MOCVD Growth of CdTe directly on $LiTaO_3$**

A program is currently under way in collaboration with Telecom Research Laboratory. Their MOCVD machine has been used to deposit CdTe directly onto a $LiTaO_3$ substrate. The aim of the work is to try to integrate an optoelectronic switch with the electro-optic substrate. This, of course, can be achieved directly with GaAs (since GaAs is an electro-optic crystal), however the sampling pulse has to be in the near infra-red and as such cannot be used with our laser system as it is presently configured. It has proved difficult to get the CdTe to bond to the $LiTaO_3$, and so the sample was sent to ANU to have the CdTe "ion-stitched" to the $LiTaO_3$ substrate. This has been achieved and the new samples are ready for electrode fabrication by Microelectronics Section.

6 CONCLUSIONS

This report details the construction and performance of an ultrafast electro-optic sampling system suitable for instrumental applications, which operates in a manner similar to that of most multi-gigahertz digitising oscilloscopes or vector network analysers.

The system is predicted to have an aperture time of about 300 fs, which implies a sampling bandwidth easily exceeding 300 GHz for repetitive sampling of periodic signals. Other system parameters were found to be:

(i) an estimated worst-case sensitivity of -20 dBm (across 0 - 20 GHz)
(ii) an estimated worst-case total system insertion loss of 74 dB (associated with electrical to optical to electrical conversion by the modulator, photodiode detectors and lockin amplifier)
(iii) a dynamic range in excess of 60 dB.

The modulator itself was measured to have a 10 dB forward transmission loss, which appears to be mainly attributable to losses associated with the transitions between the various propagation modes necessary to get the signal onto and off the modulator. The modal evolution is also probably the major source of pulse dispersion.

Comparison of the electro-optically sampled version of a test signal with that obtained using an 18 GHz sampling oscilloscope demonstrated the superior signal to noise ratio attainable with the electro-optic technique. Minor discrepancies between the ratios of various features in the test signal as recorded by the two techniques are tentatively attributable to the combined effects of:

(i) significant dispersion and multiple reflections of the test signal as it propagates off the modulator structure, due to the transition from a coplanar stripline mode to a coplanar waveguide mode to a coaxial mode. This will alter the signal recorded by the oscilloscope; and
(ii) the effect of approximately 20 ps of timing jitter to which the oscilloscope is subject but the electro-optic system is not.

Finally, in Section 5 some applications for the system were outlined, along with a brief summary of current collaborative research involving Telecom Research Laboratory, the Australian National University and the CSIRO Division of Radiophysics.

REFERENCES

1 Valdmanis, J.A., Morou, G.A. and Gabel, C.W., "Subpicosecond Electrical Sampling", IEEE J. Quant. Elec. **QE-19**, pp 664-7, 1983.

2 Fork, R.L., Brito Cruz, C.H., Becker, P.C. and Shank, C.V., "Compression of optical pulses to six femtoseconds by using cubic phase compensation", Opt. Lett. **12**, pp 483-5, 1987.

3 Neal J. and Surber, J., "Flash Converters Work Better with Track/Holds", Analog Dialog **18**, pp 10 - 14, 1984.

4 Frankel, M.Y., Gupta, S., Valdmanis, J.A. and Morou, G.A., "Terahertz Attenuation and Dispersion Characteristics of Coplanar Transmission Lines", IEEE Trans. Mic. Theor. Tech. **MTT-39**, pp 910 - 6, 1991.

5 Gupta, K.C., Garg, R. and Bahl, I.J., *Microstrip Lines and Slotlines* (Artech House: Norwood, MA), pp 275 - 80, 1979.

6 Ramer, O.G., "Integrated Optic Electrooptic Modulator Electrode Analysis", IEEE J. Quant Elec. **QE-18**, pp 386-92, 1982.

7 Wolf, P., Van Zeghbroek, B.J. and Deutsch, U., "A Josephson Sampler with 2.1 ps Resolution", IEEE Tans. Mag. **MAG-21**, pp 226 - 9, 1985.

8 Marsland, R.A., Madden, C.J., Van der Weide, D.W., Shakouri, M.S. and Bloom, D.M., "Monolithic Integrated Circuits for MM-Wave Instrumentation", GaAS Symp., pp 19 - 22, 1990.

9 Robertson, W.M., Arjavalingam, G. and Kopcsay, G.V., "Broadband Microwave Dielectric Properties of Lithium Niobate", Elect. Lett. **27**, pp 175 - 6, 1990.

10 Gupta, S., Pamulapati, J., Chwalek, J., Bhattacharya, P.K. and Morou, G., "Subpicosecond Photoconductivity in III-V Compund Semiconductors Using Low Temperature MBE GrowthTechniques", *Ultrafast Phenomena VII* (Springer-Verlag: Berlin), pp 297 - 9, 1990.

11 Chin, S.L., *Fundamentals of Laser Optoelectronics* (World Scientific: Singapore), 1989.

APPENDIX A

PRINCIPALS OF OPERATION OF THE ELECTRO-OPTIC MODULATOR

In this appendix the basic theory of operation of the electro-optic modulator is derived. Under the influence of an electric field some materials exhibit a change in their refractive index which is linearly proportional to the applied field - a phenomenon known as the linear electro-optic effect.

If x_1, x_2 and x_3 define the principal axes of such a crystal, with associated refractive indices n_1, n_2 and n_3, then the general index ellipsoid under the influence of the applied field can be written in the form [11]

$$\frac{x_1^2}{n_1^2} + \frac{x_2^2}{n_2^2} + \frac{x_3^2}{n_3^2} + M = 1 \qquad \text{(A1)}$$

where

$$M \equiv [x_1^2, x_2^2, x_3^2, 2x_2x_3, 2x_1x_3, 2x_1x_2] \begin{pmatrix} r_{11} & r_{12} & r_{13} \\ \vdots & \vdots & \vdots \\ r_{61} & r_{62} & r_{63} \end{pmatrix} \begin{bmatrix} E_1 \\ E_2 \\ E_3 \end{bmatrix} \qquad \text{(A2)}$$

and the E_i represent the components of the applied field.

For $LiTaO_3$,

$n_1 = n_2 = n_o = 2.173$ at 648 nm
$n_3 = n_e = 2.177$ at 688 nm
$r_{51} = r_{42} = 20.0 \times 10^{-12}$ m/V
$r_{13} = r_{23} = 7.0 \times 10^{-12}$ m/V
$r_{33} = 30.3 \times 10^{-12}$ m/V

with all other $r_{ij} = 0$. The r_{ij} represent the electro-optic tensor coefficients which describe the variation in the refractive index of the crystal as a function of applied electric field.

The coplanar stripline configuration creates a field such that only E_3 is non-zero. In this case Equation (A1) can be written

$$\frac{x_1^2}{n_o'^2} + \frac{x_2^2}{n_o'^2} + \frac{x_3^2}{n_e'^2} = 1 \qquad \text{(A3)}$$

where

$$n'_o \equiv \frac{n_o}{(1 + r_{13}\, n_o^2\, E_3)^{1/2}} \tag{A4}$$

$$n'_e \equiv \frac{n_e}{(1 + r_{33}\, n_e^2\, E_3)^{1/2}} \tag{A5}$$

From the form of Equations (A4) and (A5) it is apparent that the general form for the change in the refractive index can be written

$$\Delta n = \frac{-r\, n^3\, E_3}{2} \tag{A6}$$

where $r=r_{13}$ when $n=n_o$, and $r=r_{33}$ when $n=n_e$. Since E_3 is time dependent, both the ordinary and extraordinary components of the crystal refractive index will reflect variations in the amplitude of the electrical signal.

In order to clarify the process of converting the refractive index variation into an intensity variation of an optical beam penetrating the crystal it is useful to employ a Jones matrix formalism [11]. In this case the two coordinate axes for the calculation are defined to be parallel and orthogonal to the polarisation of the input laser beam, and the electric field is normalised to unity.

An analysis of the optical arrangement shown in Figure 1 - the first polariser defining the input polarisation; the electro-optic modulator and Soleil-Babinet compensator with their principal axes aligned and at 45° to the input beam; and a final polariser orthogonal to the input polariser (this final polariser is usually called the *analyser*) - gives for the output electric field of the laser

$$E_{out}(t) = A\, R(-45)\, M(t)\, R(45)\, E_{in} \tag{A7}$$

where

$$E_{in} = \begin{pmatrix} 1 \\ 0 \end{pmatrix} \text{ - input electric field} \tag{A8}$$

$$R(45) = \frac{1}{\sqrt{2}} \begin{pmatrix} 1 & 1 \\ -1 & 1 \end{pmatrix} \text{ - rotation to modulator optical axes} \tag{A9}$$

$$M(t) = \begin{pmatrix} e^{-ik_o(t)d} & 0 \\ 0 & e^{-ik_e(t)d} \end{pmatrix} \text{ - phase shift matrix} \tag{A10}$$

$$R(-45) = \frac{1}{\sqrt{2}}\begin{pmatrix} 1 & -1 \\ 1 & 1 \end{pmatrix} \text{ - rotation back to original axes} \qquad (A11)$$

$$A = \begin{pmatrix} 0 & 0 \\ 0 & 1 \end{pmatrix} \text{ - analyser} \qquad (A12)$$

The phase matrix M(t) describes the phase variations imposed upon the ordinary and extraordinary components of the laser as it propagates through the modulator and the SBC. The wavenumber elements k_o and k_e (defined by $k_i = 2\pi/\lambda_i$, i=o, e) reflect both the time varying signal modulation and the static birefringence of the $LiTaO_3$ and SBC. The distance d is the total propagation distance of the beam through these two elements. It is useful to define the total relative phase shift ε_p via

$$\varepsilon_p(t) = \varepsilon_s + \varepsilon(t) = (k_o(t) - k_e(t))d \qquad (A13)$$

where ε_s and $\varepsilon(t)$ represent the static and time-varying contributions. Furthermore, defining the average phase shift as

$$\phi(t) = \frac{(k_o(t) + k_e(t))d}{2} \qquad (A14)$$

allows the phase matrix M(t) to be written as

$$M(t) = e^{-i\phi(t)}\begin{bmatrix} e^{-i\varepsilon_p(t)/2} & 0 \\ 0 & e^{i\varepsilon_p(t)/2} \end{bmatrix} \qquad (A15)$$

Substituting Equation (A15) into (A7) and carrying out the matrix multiplications yields

$$E_{out} = -ie^{-i\phi(t)} \sin\frac{\varepsilon_p(t)}{2}\begin{pmatrix} 0 \\ 1 \end{pmatrix} \qquad (A16)$$

where the column vector simply indicates a polarisation state orthogonal to the original input beam, as defined by Equation (A8). The fraction of transmitted power is

$$\begin{aligned} S &= \frac{E_{out}^A E_{out}}{E_{in}^A E_{in}} \qquad (E^A \text{ stands for the adjoint of E}) \\ &= \sin^2\left(\frac{\varepsilon_p(t)}{2}\right) \\ &= \sin^2\left(\frac{\varepsilon_s}{2} + \frac{\varepsilon(t)}{2}\right) \\ &= \frac{1}{2}\left[1 - \cos\varepsilon_s \cos\varepsilon(t) + \sin\varepsilon_s \sin\varepsilon(t)\right] \end{aligned} \qquad (A17)$$

Equation (A17) describes the generalised response of the modulator for arbitrary static relative phase shift ε_s. The two contributions to ε_s arise from the birefringence of the $LiTaO_3$ ($n_o - n_e = -0.004$), and from the tunable birefringence of the SBC. If the total relative phase

shift is $\frac{\pi}{2}$ (ie the $LiTaO_3$ and SBC combined form a quarter wave plate), then the transmitted intensity varies as

$$S = \frac{1}{2}[1 + \sin \varepsilon(t)] \tag{A18}$$

which, for small phase variations, reduces to

$$S = \frac{1}{2}[1 + \varepsilon(t)] \tag{A19}$$

where, from Equations (A6), (A13) and for $n_o \sim n_e$

$$|\varepsilon(t)| = \frac{\pi}{\lambda}(r_{33} - r_{13})\, n_e^3\, E_3(t) d \tag{A20}$$

From equation (A18), the maximum transmitted signal ocurrs when

$$\begin{aligned} |\varepsilon(t)| &= \frac{\pi}{2} = \frac{\pi}{\lambda}(r_{33} - r_{13})\, n_e^3\, E_3^{max} d \\ \Rightarrow E_3^{max} d &= \frac{\lambda}{2(r_{33} - r_{13})\, n_e^3} \equiv \frac{V_\pi}{2} \end{aligned} \tag{A21}$$

Equation (A21) defines the voltage V_π required to fully switch the modulator from zero transmission to full transmission. The quantity V_π is a fundamental parameter in the design and analysis of any electro-optic modulator configuration.

DISTRIBUTION

	Copy No.
Defence Science and Technology Organisation	
Chief Defence Scientist)	
Central Office Executive)	1
Counsellor, Defence Science, London	Cont Sht
Counsellor, Defence Science, Washington	Cont Sht
Scientific Adviser, Defence Central	1
Navy Scientific Adviser	1
Air Force Scientific Adviser	1
Scientific Adviser, Army	1
ADT, Building N,Russell Offices	1
Electronics Research Laboratory	
Director	1
Chief, Communications Division	1
Chief, Information Technology Division	Cont Sht
Chief, Electronic Warfare Division	1
Research Leader, Signal Information Processing	1
Research Leader, Secure Communications	1
Head, Electronic Warfare Technology	1
Dr A.C. Lindsay (co-Author)	1
G.A. Knight (co-Author)	1
S.C. Troedson (co-Author)	1
Media Services	1
Libraries and Information Services	
Australian Government Publishing Service	1
Defence Central Library, Technical Reports Centre	1
Manager, Document Exchange Centre, (for retention)	1
National Technical Information Service, United States	2
Defence Research Information Centre, United Kingdom	2
Director Scientific Information Services, Canada	1
Ministry of Defence, New Zealand	1
National Library of Australia	1
Defence Science and Technology Organisation Salisbury, Research Library	2
Library Defence Signals Directorate, Melbourne	1
British Library Document Supply Centre	1
Defence Intelligence Organisation Research Service	1
Spares	
Defence Science and Technology Organisation Salisbury, Research Library	6

Department of Defence

DOCUMENT CONTROL DATA SHEET

Page Classification
UNCLASSIFIED
Privacy Marking/Caveat (of Document)
N/A

1a. AR Number	1b. Establishment Number	2. Document Date	3 Task Number
AR-008-114	ERL-0673-RR	February 1993	DEF 89/210

4. Title	5. Security Classification	6. No. of Pages	44
ELECTRO-OPTIC CHARACTERISATION OF EXTREMELY WIDE BANDWIDTH ELECTRICAL SIGNALS	U (Document) U (Title) U (Abstract)	7. No. of Refs.	11

S (Secret) C (Confi.) R (Rest) U (Unclass)

* For UNCLASSIFIED docs with a secondary distribution LIMITATION, use (L) in document box.

8. Author(s)	9. Downgrading/Delimiting Instructions
A.C. Lindsay, G.A. Knight, S.C. Troedson and I.G. Fuss	N/A

10a. Corporate Author and Address	11. Officer/Position responsible for
Electronics Research Laboratory PO Box 1500 SALISBURY SA 5108	Security..... Downgrading..... Approval for Release.....DERL.....
10b. Task Sponsor DEF	

12. Secondary Distribution of this Document

APPROVED FOR PUBLIC RELEASE

Any enquiries outside stated limitations should be referred through DSTIC, Defence Information Services, Department of Defence, Anzac Park West, Canberra, ACT 2600.

13a. Deliberate Announcement

No limitation

13b. Casual Announcement (for citation in other documents)

[√] No Limitation

[ ] Ref. by Author, Doc No. and date only.

14. DEFTEST Descriptors	15. DISCAT Subject Codes
Signal Processing, Bandwidth, Frequencies, Oscilloscopes	090102

16. Abstract

In this report an ultrafast electro-optic sampling system suitable for applications such as device characterisation is described. The aperture time of the sampler is calculated to be about 290 fs, implying an attainable device bandwidth in excess of 300 GHz. The sampler was characterised using a test pulse with approximately 12 GHz of frequency content, and the results compared to those obtained from an 18 GHz digital sampling oscilloscope.

Doc.Sect WF11

Page Classification

UNCLASSIFIED

16. Abstract (CONT.)

17. Imprint

Electronics Research Laboratory
PO Box 1500
SALISBURY SA 5108

18. Document Series and Number	19. Cost Code	20. Type of Report and Period Covered
ERL-0673-RR	723238	RESEARCH REPORT

21. Computer Programs Used

N/A

22. Establishment File Reference(s)

N/A

23. Additional information (if required)

Doc.Sect WF11